

# Partial volume correction for volume estimation of liver metastases and lymph nodes in CT scans using spatial subdivision

Frank Heckel<sup>a</sup>, Volker Dicken<sup>a</sup>, Tilman Bostel<sup>b</sup>, Michael Fabel<sup>c</sup>, Andreas Kießling<sup>d</sup> and Heinz-Otto Peitgen<sup>a</sup>

<sup>a</sup>Fraunhofer MEVIS, Bremen, Germany;

<sup>b</sup>Johannes Gutenberg University, Clinic and Out-patients' Clinic for Diagnostic and Interventional Radiology, Mainz, Germany;

<sup>c</sup>Christian-Albrechts-University, Department of Diagnostic Radiology, Kiel, Germany;

<sup>d</sup>Philipps-University, Department of Diagnostic Radiology, Marburg, Germany

## ABSTRACT

In oncological therapy monitoring, the estimation of tumor growth from consecutive CT scans is an important aspect in deciding whether the given treatment is adequate for the patient. This can be done by measuring and comparing the volume of a lesion in the scans based on a segmentation. However, simply counting the voxels within the segmentation mask can lead to significant differences in the volume, if the lesion has been segmented slightly differently by various readers or in different scans, due to the limited spatial resolution of CT and due to partial volume effects.

We present a novel algorithm for measuring the volume of liver metastases and lymph nodes which considers partial volume effects at the surface of a lesion. Our algorithm is based on a spatial subdivision of the segmentation. We have evaluated the algorithm on a phantom and a multi-reader study. Our evaluations have shown that our algorithm allows determining the volume more accurately even for larger slice thicknesses. Moreover, it reduces inter-observer variability of volume measurements significantly. The calculation of the volume takes 2 seconds for  $50^3$  voxels on a single 2.66GHz Intel Core2 CPU.

**Keywords:** Classification, Statistical methods, Quantification, Volume, Partial volume effect, Partial volume artifacts, Partial volume correction, Measurement

## 1. INTRODUCTION

In oncological therapy monitoring, the estimation of tumor growth from consecutive CT scans is an important aspect in deciding whether the given treatment is adequate for the patient. According to the current RECIST<sup>1</sup> standard this is done in terms of the maximum axial diameter. In RECIST a 30% decrease in the sum of diameters of the target lesions\* is defined as a partial response, while an increase of 20% is classified as progressive disease. However, recent advances in medical image processing allow measuring the volume of a lesion in the scans which has the potential to be more accurate and reproducible than the diameter measurement.<sup>2</sup> Thus, automatic segmentation and volumetry increase reliability and significance of monitoring tumor growth in follow-up examinations.<sup>3</sup> Unfortunately, response and progress are clinically not yet defined for volume measurements.

For determining the volume of a lesion it needs to be segmented. Because manual segmentation is time-consuming and error-prone, automatic segmentation algorithms followed by a manual correction might be used. Based on the segmentation the volume of the lesion can be measured. However, simply counting the voxels within the segmentation mask can lead to significant differences in the volume, if the lesion has been segmented slightly differently by various readers or in different scans, acquired with different scan parameters such as the

---

Further author information: (Send correspondence to F. Heckel.)

F. Heckel: E-mail: frank.heckel@mevis.fraunhofer.de, Telephone: +49 (0)421 218 9068

\**Lesion* refers to both liver metastases and lymph nodes in this context.

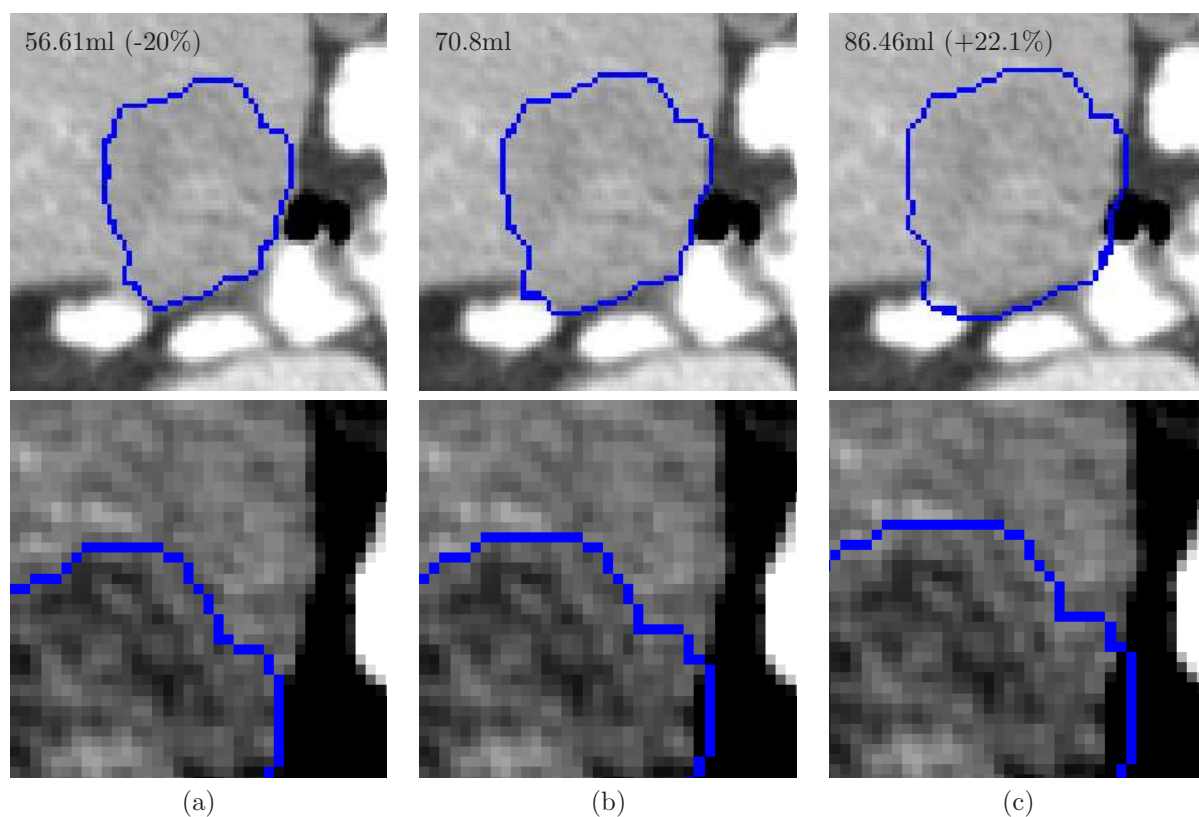


Figure 1. Naive voxel-count-volume and relative difference to the ground truth segmentation for various segmentations (blue line) of a liver metastasis (the blue voxels themselves are not part of the segmentation): (a) a slightly eroded segmentation, (b) the ground truth segmentation, (c) a slightly dilated segmentation. Notice, that each segmentation might be accepted as a proper segmentation by various readers, especially at the border to the liver tissue, which you can see in the bottom row where the contrast of the images has been adapted to better show the border between the metastasis and the tissue.

voxel size or the reconstruction kernel. Reasons for this can be the limited spatial resolution of CT, noise in the images and partial volume effects. In addition, counting voxels does not result in the real physical volume of the lesion due to partial volume artifacts. Partial volume artifacts appear at the border between objects, because a voxel might represent more than one tissue there, i.e. the value of a voxel is a mixture of two or more tissues. Figure 1 shows this on the example of a liver metastasis where the ground truth segmentation of a tumor has been slightly eroded and dilated using a  $3 \times 3 \times 3$  kernel resulting in about one removed (resp. added) “voxel layer”. Depending on the reader and the windowing settings used for segmentation, each of the results in this example might be accepted as a proper segmentation of the tumor. However, the volume difference of about 20% might already be rated as progress or response when dealing with follow-up examinations. Hence, the diagnosis might change only depending on the inter-<sup>†</sup> or intra-observer variability<sup>‡</sup>, which is not acceptable.

Most work in partial volume correction focuses on MR and PET where the whole dataset is being corrected.<sup>4-6</sup> Other authors focus on brain lesions in MR.<sup>7,8</sup> An algorithm for volume calculation of lung nodules in CT with partial volume correction has been developed by Kuhnigk *et al.*<sup>9</sup> Volumetric quantification of plaque in CT considering partial volume effects has been presented by Dehmeshki *et al.*<sup>10</sup> Common approaches for partial volume correction are Bayesian classification, histograms and statistical as well as mixture models. All these algorithms cannot be used adequately for estimating the volume of liver metastases or lymph nodes because of the multiple tissues surrounding such lesions or because of their calculation times. Furthermore, we do not want

<sup>†</sup>The *inter-observer variability* measures the differences of measurements by different readers.

<sup>‡</sup>The *intra-observer variability* measures the differences of measurements by the same reader.

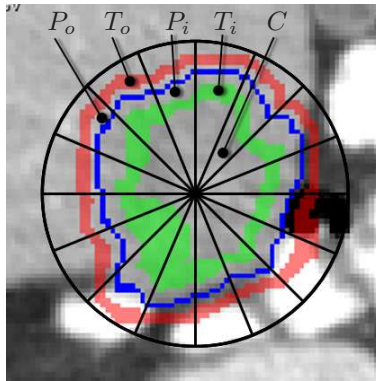


Figure 2. Spatial subdivision for partial volume correction: initial segmentation (blue), inner tissue  $T_i$  (green), outer tissue  $T_o$  (red) and the segments of the spatial subdivision (black). The inner and outer partial volume areas  $P_i$  and  $P_o$  are the transparent areas between the segmentation and the inner and the outer tissue respectively. The lesion core  $C$  is the part inside the inner tissue. For simplicity the segments are shown in 2D. The blue voxels surrounding the segmentation are not part of the segmentation itself.

to compensate the partial volume effect for the image data, but our goal is to consider it when calculating the volume of a tumor based on its segmentation.

In this paper we present a novel algorithm for measuring the volume of liver metastases and lymph nodes which considers partial volume effects at the surface of a lesion based on a spatial subdivision. Therefore, it is able to take different tissues around the lesion into account. By considering partial volume effects the volume can be determined more accurately even for larger slice thicknesses. Moreover, it reduces inter-observer variability of volume measurements significantly.

## 2. METHOD

Our algorithm is based on the assumption that partial volume voxels are located at the border between the lesion and the surrounding tissue and that the values of these voxels are a mixture of the tissue inside and outside the lesion. We assume that a partial volume voxel is a linear combination of exactly two tissues here.

For taking partial volume effects at the surface of the segmentation into account while calculating the volume of a lesion, we define five areas based on the initial segmentation (see Fig. 2):

- The *lesion core*  $C$ , which is given by two erosions of the initial segmentation with a spherical  $5 \times 5 \times 5$  kernel.
- The *inner tissue* area  $T_i$ , which defines the tissues of the lesion. The inner tissue is given by an erosion of the initial segmentation with a spherical  $5 \times 5 \times 5$  kernel, subtracted by  $C$ .
- The *inner partial volume* area  $P_i$ , which defines the part of the lesion inside the segmentation that is affected by partial volume artifacts. This area is given by subtracting  $T_i \cup C$  from the initial segmentation.
- The *outer partial volume* area  $P_o$ , which defines the part of the lesion outside the segmentation that is affected by partial volume artifacts. This area is given by a dilation of the initial segmentation with a spherical  $5 \times 5 \times 5$  kernel, from which the initial segmentation is subtracted.
- The *outer tissue* area  $T_o$ , which defines the tissues of the objects surrounding the lesion. The outer tissue is given by two dilations of the initial segmentation with a spherical  $5 \times 5 \times 5$  kernel, subtracted by  $P_o$  and the initial segmentation.

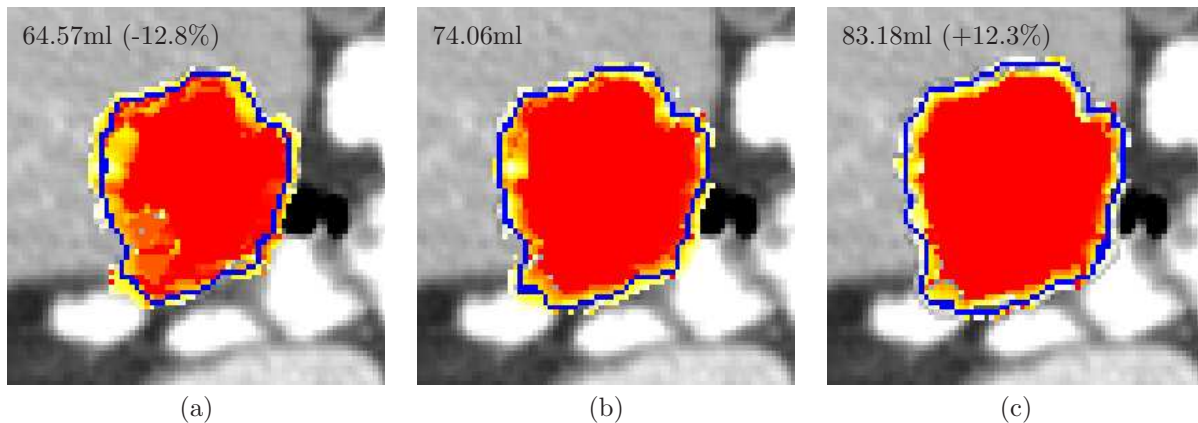


Figure 3. Volume estimation using our algorithm for different segmentations (blue line) of a liver metastasis: (a) a slightly eroded segmentation, (b) the ground truth segmentation, (c) a slightly dilated segmentation. The relative difference to the ground truth segmentation is given in parentheses. The weight of each voxel is overlaid with red = 1, orange = 0.75, yellow = 0.5, white = 0.25 and transparent=0.0. Notice the border of the segmentation, where voxels in (a) have a higher weight and voxels in (c) have a lower weight compared to (b).

Because there are typically various structures around a liver metastasis or a lymph node, we subdivide the lesion into several segments. The subdivision of the volume is done into three-dimensional equiangular parts with the center of those parts being at the center of gravity of the segmentation (see Fig. 2). We assume that the lesion is an ellipsoidal, compact object here, so there are no overlapping parts of the surface in each segment and the subdivision is rather uniform.

Using the tissue areas and the subdivision, the algorithm for calculating the weights of each voxel within the partial volume areas is as follows:

1. For each segment  $S$  of the subdivision:
  - (a) Calculate the average outer tissue value  $t_o$  of  $T_o \cap S$
  - (b) Calculate the average inner tissue value  $t_i$  of  $T_i \cap S$
  - (c) For each voxel  $V$  of the inner partial volume area  $P_i \cap S$  with gray value  $v$ :
    - i. Calculate the voxel's weight  $w_V$  based on  $v$  as linear combination of  $t_o$  and  $t_i$  (see Eq. 1)
  - (d) For each voxel  $V$  of the outer partial volume area  $P_o \cap S$  with gray value  $v$ :
    - i. If the average value  $p_o$  of the outer partial volume area equals  $t_o$  set  $w_V = 0$ , because we assume that this part has intentionally been cut away (which can be the case for confluent lesions), otherwise:
      - ii. Calculate the voxel's weight  $w_V$  based on  $v$  as linear combination of  $t_o$  and  $t_i$  (see Eq. 1)

The weight of each voxel is clamped to  $[0, 1]$  because values outside this range are typically a result of noise. Therefore, the weight is calculated as follows:

$$w_V = \begin{cases} 0, & \text{if } \frac{t_o - v}{t_o - t_i} < 0 \\ \frac{t_o - v}{t_o - t_i}, & \text{if } 0 \leq \frac{t_o - v}{t_o - t_i} \leq 1 \\ 1, & \text{if } \frac{t_o - v}{t_o - t_i} > 1 \end{cases} \quad (1)$$

The average tissue values are calculated as the median of all gray values within a tissue area of a given segment. The weights of the voxels within the inner tissue and the lesion core are set to 1. The outer tissue is weighted by 0.

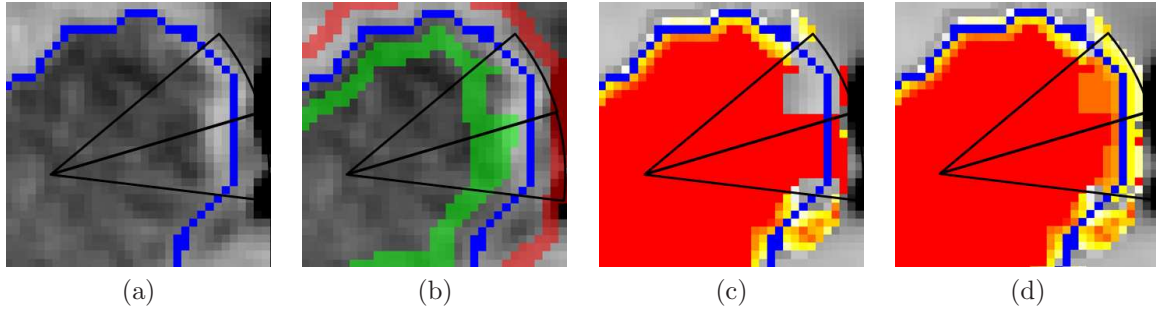


Figure 4. A special case where the weight calculation using Eq. 1 fails because the inner and outer tissue areas do not represent the tissues that influence the partial volume areas. The relevant segments are indicated in black (note that these are not the real segments used for computation, which are actually three-dimensional). (a) shows the segmentation and (b) shows the inner and outer tissue areas. Using Eq. 1 the weight calculation for some voxels fails (c). Using the fallback described in Eq. 4 the weights are more plausible (d).

The volume  $\text{Vol}_L$  of a lesion is given by summing up the volumes  $\text{Vol}_V$  of each voxel of the lesion core, the inner tissue and the inner and outer partial volume areas, weighted by  $w$  (see Fig. 3):

$$\text{Vol}_L = \sum_{V \in L} w_V * \text{Vol}_V, L = C \cup T_i \cup P_i \cup P_o \quad (2)$$

For compensation of noise all computations are done on a smoothed dataset. For smoothing a  $5 \times 5 \times 5$  Gauss-kernel is used. Moreover, the dataset is supersampled using a trilinear filter such that the voxels are isotropic (i.e. cubic). Supersampling is necessary in order to have enough voxels in each segment to be able to calculate valid average values for each segment.

## 2.1 Special Cases

There are two special cases that need to be treated differently from the general algorithm described in the previous section.

If the lesion is small then segments of the inner tissue area  $T_i$  might not contain enough voxels for calculating an accurate average tissue value. Moreover, the lesion core  $C$  might be empty. A lesion is considered too small if  $|T_i| < 5 \cdot |S|$ , where  $|T_i|$  is the number of voxel within  $T_i$  and  $|S|$  is the number of segments. In this case the average lesion core value  $c$  is used instead of  $t_i$  in Eq. 1, where  $c$  is given by the median of the voxels within both the lesion core and the inner tissue  $C \cup T_i$ .

$$w_V = \begin{cases} 0, & \text{if } \frac{t_o - v}{t_o - c} < 0 \\ \frac{t_o - v}{t_o - c}, & \text{if } 0 \leq \frac{t_o - v}{t_o - c} \leq 1 \\ 1, & \text{if } \frac{t_o - v}{t_o - c} > 1 \end{cases} \quad (3)$$

Another special case are segments  $S$  where the values of the voxels are not in the range between the average values of the inner and the outer tissue, i.e. voxel with weights  $\ll 0$  or  $\gg 1$  according to Eq. 1. This is the case if  $T_o \cap S$  and  $T_i \cap S$  do not represent the tissues which have an influence on the partial volume effect of the voxels in  $P_i \cap S$  and  $P_o \cap S$  (see Fig. 4). In this case the weights  $w_V$  of such voxels are calculated based on their distance  $d_V$  to the surface of the inner tissue area instead, with  $d_{\max}$  being the maximum distance to  $T_i$  of any voxel  $V \in P_o \cup P_i$ :

$$w_V = 1 - \frac{d_V}{d_{\max}} \quad (4)$$

In our test cases thresholds of  $-0.25$  and  $1.25$  have shown to be a good choice for deciding whether to use Eq. 1 or Eq. 4.

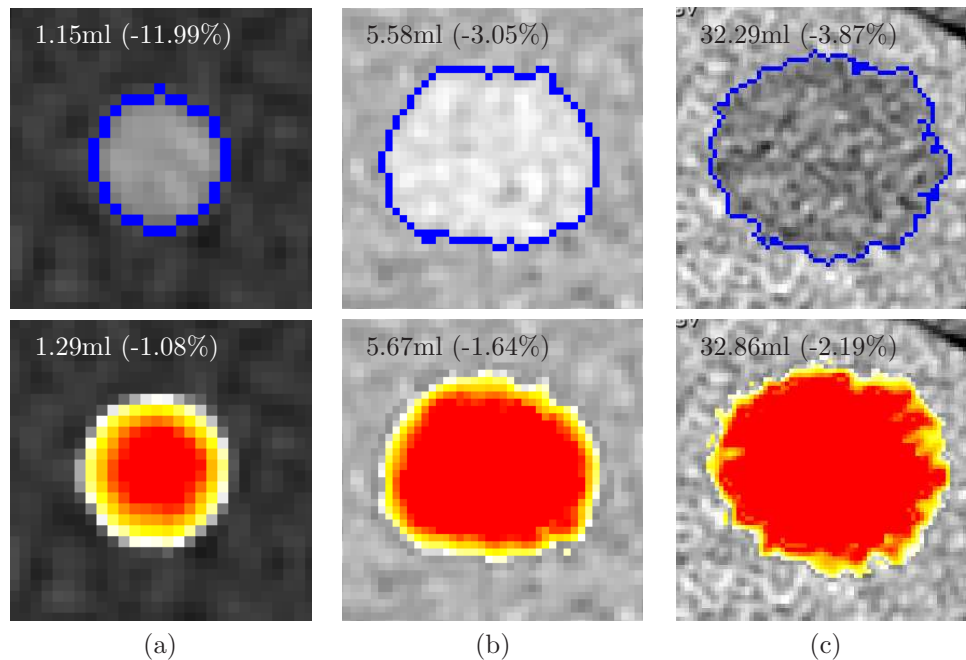


Figure 5. Examples of the evaluation on the 1mm B30 phantom. The top row shows the initial segmentation and the voxel-count-volume, the bottom row shows the result of our algorithm. For each example the difference to the real volume is given in parentheses. (a) shows a lymph node phantom, (b) is a phantom of a hyperdense liver metastasis while (c) is a phantom of a hypodense liver metastasis.

### 3. RESULTS

We have evaluated our algorithm on a physical phantom<sup>§</sup> containing 31 lesions (7 hyper- and 7 hypodense liver metastases as well as 17 lymph nodes) with volumes between 0.23ml and 52.36ml. The phantom is constructed such that the lesions and the tissues are homogeneous and that a lesion is surrounded by only one type of tissue. Some examples are given in Fig. 5. The phantom dataset has been reconstructed using various slice thicknesses and kernels. Segmentation was done using an automatic algorithm that was developed by Moltz *et al.*<sup>2</sup> Based in this segmentation the naive volume was calculated by counting the voxels within the segmentation mask, multiplied by the volume of one voxel, and the corrected volume was calculated using our algorithm. For simulating inter-observer variability we also calculated the volume of an eroded and a dilated segmentation using a  $3 \times 3 \times 3$  Kernel resulting in about one removed (resp. added) “voxel layer”. The results are given in Tab. 1, where the average relative difference and the standard deviation of the calculated volumes to the real volumes are shown. The average represents systematical errors, while the standard deviation is a measure for the reliability of the calculated volume. As can be seen, using partial volume correction, the volume can be calculated more accurately for most of the lesions or the error is at least in the same order as the error of the voxel-count volume. Moreover, the standard deviation is decreased for all datasets. Furthermore, slight over- and undersegmentations are compensated by the algorithm. The results of the 5mm datasets suggest that the lesions have systematically been oversegmented which needs to be further investigated.

Finally we have evaluated the inter-observer variability based on 132 liver metastases, that have been segmented by two radiologists (see Tab. 2). Segmentation was done using the algorithm by Moltz *et al.*,<sup>2</sup> followed by a manual correction developed by Heckel *et al.*<sup>11</sup> The dataset has been collected from several clinics and CT scanners. Rim-enhancing metastases have been excluded from this evaluation, which is further discussed in Sec. 4. The difference between the readers is compensated by our algorithm, resulting in a more robust and reproducible volume measurement. Figure 6 shows an example of this study.

<sup>§</sup>The phantom data was provided by Siemens AG Healthcare Sector Imaging & IT Division Computed Tomography, Forchheim.

Table 1. Results of our phantom evaluation on 31 lesions (9 lesions <2ml, 13 lesions 2-10ml, 9 lesions >10ml). The table shows the average relative differences to the real volume of the lesions in percent for both the voxel-count volume and the volume with partial volume correction using our algorithm. The standard deviation in percent is given in parentheses.

Size	Dataset	Initial		Eroded		Dilated	
		Voxel-count	Corrected	Voxel-count	Corrected	Voxel-count	Corrected
<2ml	1mm, B30	-3.0 (11.0)	1.9 (5.5)	-58.2 (6.9)	-15.2 (6.0)	80.7 (40.7)	22.6 (16.3)
	1mm, B40	-2.1 (10.8)	1.8 (7.0)	-57.9 (7.1)	-15.9 (7.2)	82.5 (40.1)	26.3 (18.5)
	2mm, B30	-0.6 (16.7)	1.8 (6.6)	-59.1 (4.9)	-15.7 (9.0)	89.7 (55.8)	26.0 (18.7)
	2mm, B40	0.7 (16.5)	2.7 (7.4)	-58.6 (5.2)	-14.9 (8.6)	91.9 (55.6)	27.3 (20.0)
	3mm, B30	5.6 (22.5)	6.4 (14.0)	-56.8 (4.6)	-14.8 (12.6)	101.1 (63.6)	36.5 (29.1)
	3mm, B40	4.4 (22.4)	5.0 (11.4)	-56.4 (4.7)	-15.6 (11.8)	98.3 (65.4)	34.5 (26.1)
	4mm, B30	12.5 (37.9)	9.8 (21.1)	-53.9 (9.8)	-15.7 (16.4)	112.7 (88.8)	44.9 (39.5)
	4mm, B40	13.5 (39.4)	10.3 (21.5)	-53.7 (10.2)	-15.1 (16.3)	115.2 (92.8)	45.0 (40.0)
	5mm, B30	36.2 (51.1)	27.4 (24.9)	-41.1 (13.8)	-2.6 (19.3)	151.1 (115.5)	70.7 (46.4)
5mm, B40	35.4 (51.7)	26.9 (24.6)	-41.5 (14.5)	-3.3 (19.6)	150.2 (116.2)	69.3 (46.0)	
2-10ml	1mm, B30	-3.1 (4.4)	-0.1 (1.5)	-36.8 (7.1)	-10.8 (6.2)	37.4 (10.8)	11.0 (9.5)
	1mm, B40	-2.8 (4.0)	0.0 (1.2)	-36.6 (6.5)	-11.1 (5.8)	37.9 (10.6)	13.2 (9.7)
	2mm, B30	-4.9 (2.9)	-0.8 (1.7)	-37.9 (5.5)	-11.9 (4.1)	35.7 (7.3)	9.9 (5.4)
	2mm, B40	-5.3 (3.4)	-0.9 (1.6)	-38.3 (6.3)	-12.2 (5.3)	35.4 (7.0)	9.6 (4.7)
	3mm, B30	-6.7 (4.1)	-1.7 (1.6)	-38.3 (5.3)	-14.4 (4.4)	32.4 (6.7)	10.3 (3.5)
	3mm, B40	-6.8 (5.5)	-2.0 (3.0)	-38.6 (6.4)	-14.8 (6.4)	32.6 (7.8)	10.3 (3.7)
	4mm, B30	-7.5 (4.4)	-2.3 (2.3)	-38.7 (5.0)	-16.3 (4.1)	31.2 (7.1)	11.4 (3.8)
	4mm, B40	-6.4 (3.5)	-1.1 (2.6)	-38.2 (4.3)	-15.3 (2.7)	33.0 (7.3)	12.7 (6.4)
	5mm, B30	10.0 (11.4)	15.5 (10.4)	-26.2 (6.9)	-2.8 (6.0)	-54.1 (18.3)	34.7 (18.9)
5mm, B40	7.6 (8.7)	13.8 (9.9)	-27.7 (5.4)	-4.3 (4.9)	51.0 (15.0)	31.9 (17.4)	
>10ml	1mm, B30	-1.1 (1.8)	-0.4 (1.0)	-27.6 (6.4)	-9.4 (4.9)	28.7 (6.7)	9.9 (5.4)
	1mm, B40	-1.8 (2.8)	-0.6 (1.6)	-29.4 (9.5)	-12.4 (10.3)	24.1 (9.3)	7.4 (5.4)
	2mm, B30	-2.3 (2.4)	-0.7 (0.9)	-29.2 (10.7)	-12.2 (11.2)	22.5 (10.0)	5.4 (7.0)
	2mm, B40	-2.5 (2.5)	-0.8 (1.2)	-29.5 (10.5)	-12.4 (11.2)	22.6 (9.7)	5.6 (6.3)
	3mm, B30	-2.2 (2.0)	-0.9 (1.3)	-26.5 (5.7)	-9.8 (3.1)	25.9 (5.1)	9.1 (2.5)
	3mm, B40	-2.2 (2.0)	-0.9 (1.3)	-26.8 (5.9)	-9.9 (3.3)	26.1 (5.0)	9.2 (2.6)
	4mm, B30	-2.1 (2.3)	-0.8 (1.2)	-26.1 (4.6)	-10.5 (2.5)	25.7 (6.0)	9.9 (3.2)
	4mm, B40	-1.9 (2.2)	-0.6 (1.2)	-26.2 (4.9)	-10.3 (2.5)	26.2 (5.9)	10.2 (3.4)
	5mm, B30	12.2 (2.4)	13.4 (0.9)	-14.2 (5.5)	1.5 (3.2)	42.6 (6.2)	26.3 (3.1)
5mm, B40	11.8 (2.1)	13.3 (1.3)	-14.8 (5.5)	1.3 (3.3)	42.4 (5.8)	26.1 (3.2)	
All	1mm, B30	-2.5 (6.5)	0.4 (3.2)	-40.3 (13.9)	-11.7 (6.1)	47.4 (31.3)	14.1 (12.1)
	1mm, B40	-2.3 (6.3)	0.4 (3.9)	-40.7 (13.7)	-12.9 (7.8)	46.8 (32.7)	15.3 (13.9)
	2mm, B30	-2.9 (9.1)	0.0 (3.8)	-41.5 (13.9)	-13.1 (8.0)	47.5 (40.7)	13.3 (13.8)
	2mm, B40	-2.7 (9.2)	0.2 (4.3)	-41.6 (13.7)	-13.0 (8.1)	48.1 (41.3)	13.6 (14.4)
	3mm, B30	-1.8 (13.0)	0.9 (8.2)	-40.3 (12.9)	-13.2 (7.6)	50.5 (46.8)	17.5 (19.6)
	3mm, B40	-2.2 (13.0)	0.4 (6.9)	-40.4 (12.9)	-13.6 (7.9)	49.8 (46.6)	17.0 (17.8)
	4mm, B30	-0.2 (21.6)	1.6 (12.3)	-39.5 (12.6)	-14.4 (9.3)	53.3 (60.3)	20.7 (25.9)
	4mm, B40	0.7 (22.2)	2.4 (12.4)	-39.2 (12.5)	-13.8 (9.0)	54.9 (62.2)	21.3 (26.2)
	5mm, B30	18.2 (29.8)	18.4 (15.6)	-27.0 (13.7)	-1.5 (10.9)	78.9 (77.0)	42.7 (32.6)
5mm, B40	16.9 (29.9)	17.4 (15.5)	-28.0 (13.5)	-2.4 (11.0)	77.3 (77.2)	41.1 (32.1)	

Table 2. Results of our inter-observer variability evaluation on 132 liver metastases. The table shows the relative differences between reader 1 and reader 2 in percent for both the voxel-count volume and the volume with partial volume correction using our algorithm. The standard deviation in percent is given in parentheses. The size refers the voxel-count-volume based on the segmentation of reader 1.

Size	Number of lesions	Voxel-count	Corrected
<2ml	33	16.0 (33.5)	6.5 (19.4)
2-10ml	62	9.2 (16.2)	4.4 (9.2)
>10ml	37	0.8 (11.7)	0.8 (10.7)
All	132	8.5 (21.6)	3.9 (12.9)

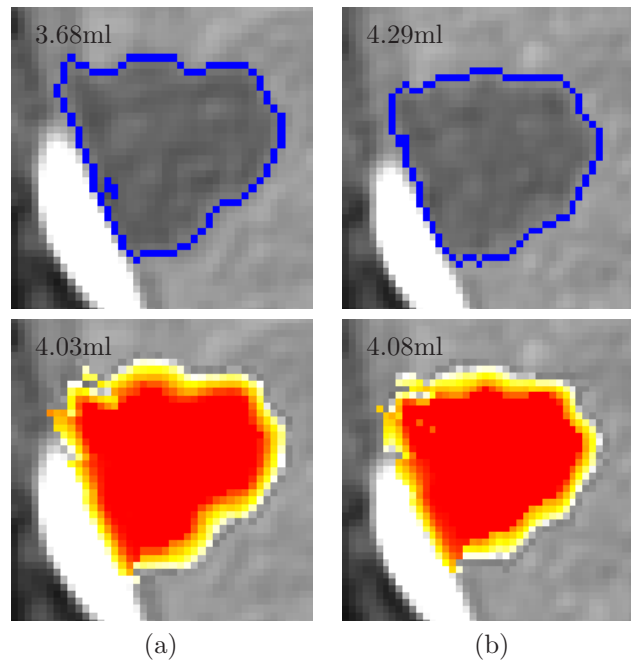


Figure 6. Two ground truth segmentations of a liver metastasis created by two radiologists ((a) and (b)). The top row shows the segmentations, the bottom row shows the result of our algorithm. The relative difference between reader (a) and reader (b) is 16.9% when using a voxel-count-volume. Using our algorithm the relative difference is 1.12%.

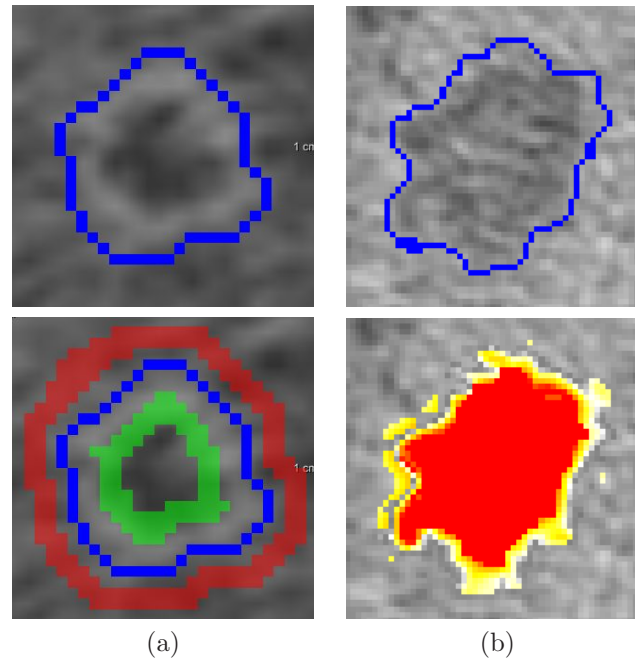


Figure 7. Problem cases for the presented algorithm: (a) shows a small rim-enhancing liver metastasis where the inner tissue area (green) does not cover the enhancement, resulting in a wrong weight calculation. (b) shows a liver metastasis where small “islands” are generated by the algorithm, which suggests that these parts should not be taken into account when calculating the volume.

The subdivision for all evaluations was done using 128 equiangular three-dimensional segments, which generates segments containing enough voxels while being accurate enough to cover appropriate tissues inside and outside of the lesion. The computation of the volume using this subdivision takes about 2 seconds for  $50^3$  voxels on a single 2.66GHz Intel Core2 CPU, which is fast enough for interactive updates of the volume measurement for example when performing manual corrections of the segmentation.

#### 4. DISCUSSION

As already discussed in the previous section, the results of our algorithm are promising. As expected, partial volume correction is more relevant for small and medium sized lesions ( $<10\text{ml}$ ), because for large lesions ( $>10\text{ml}$ ) slight differences in the segmentation have a lower relative influence on the total volume. Using partial volume correction, the volume of lesions  $<10\text{ml}$  can be estimated much more accurately and the variability between different readers is about 40-60% lower in the average and the standard deviation compared to the voxel-count-volume. For lesions  $>10\text{ml}$  the results after partial volume correction are still slightly better compared to the voxel-count-volume, especially concerning the reliability, represented by the standard deviation in Tab. 1 and Tab. 2. This means that the volume calculated using our algorithm is more reliable when comparing measurements of different readers, in different scans or at different points of time. Overall, these results demonstrate that the accuracy and reproducibility of volume assessments can be increased by the proposed algorithm.

Nevertheless, there are some open problem cases left that need further investigation. Firstly the poor results for the 5mm phantom data need to be analyzed, because this kind of data is commonly stored in a hospital’s archive. A second problem class are rim-enhancing lesions (see Fig. 7a). If the rim is small, it is not covered by the inner tissue area. As described in Sec. 2.1 the distance of each voxel to the inner tissue will be used in such cases. But because this would be done for the whole lesion, the calculated weights for the partial volume voxels and therefore the total volume are inaccurate. Such cases need to be detected and solved properly. Another problem can be seen in Fig. 7b. The presented algorithm only takes the value of each partial volume voxel into account when calculating its weight (except for the special case described in Sec. 2.1). However, this way

voxels might get a high weight although they are separated from the segmentation by voxels with a low weight, resulting in small “islands”. These separated voxels should not be taken into account when calculating the volume, because they appear not to be part of the lesion. Furthermore, the segments defined in the subdivision step might cover more than one tissue type inside and outside of the lesion, because they are evenly distributed and because they are equally sized, which can also be seen in some segments in Fig. 2. In addition there is no proper fallback if both the lesion core  $C$  the inner tissue area  $T_i$  are empty.

Using partial volume correction for measuring the volume of a lesion based on a segmentation generates a more accurate and robust result. However, using the presented algorithm the segmentation might be locally changed, i.e. voxels are added or removed from the segmentation by giving them a high or low weight. On the one hand, this is intended because the goal of the algorithm is to correct the volume based on the image data. On the other hand, this might change the segmentation generated by the clinician and voxel that are intentionally included or excluded are removed or added to the lesion. Furthermore, the calculated volume differs from the visible segmentation. Because of this inconsistency, an adaptation of the segmentation or a visualization of the corrections is necessary, which needs further research and evaluations as well.

## 5. CONCLUSION AND FUTURE WORK

The volume of a tumor in consecutive CT scans is an important parameter for deciding whether or not the given treatment is adequate for the patient. Partial volume effects can be a significant cause for variability between different clinicians and different scans, which leads to inaccurate volume measurements and which might even cause differences in diagnoses. Considering partial volume effects is challenging for liver metastases and lymph nodes because they might be surrounded by various structures.

We have presented a novel algorithm for volume estimation of liver metastases and lymph nodes that considers partial volume effects when calculating the volume. Our algorithm is fast and allows a more accurate calculation of a tumor’s volume, as demonstrated by an evaluation on physical phantom data. Moreover, a multi-reader study has shown that our algorithm is able to reduce inter-observer variability significantly. Thus, it yields potential for more robust, reproducible and reliable volume quantifications even for complex tumors. Because of its general nature, our algorithm is not restricted to liver metastases and lymph nodes and hence it can be used for other objects such as lung nodules or brain lesions as well.

Future work will aim at improving the subdivision process so each segment covers exactly one unique tissue surrounding the tumor. This should further improve the performance of our algorithm in terms of an accurate and reproducible volume measurement, because it allows a more precise determination of the voxels’ weights. Moreover, the sizes of the partial volume and the tissue areas need to be calculated adaptively for rim-enhancing liver metastases, which are not covered by the current algorithm in any case. Furthermore, we will develop a method to properly detect and handle voxels that are actually separated from the lesion itself. Finally, further evaluations of the algorithm are planned.

## ACKNOWLEDGMENT

This work was funded by Siemens AG Healthcare Sector Imaging & IT Division Computed Tomography, Forchheim.

## REFERENCES

- [1] Eisenhauer, E., Therasse, P., Bogaerts, J., Schwartz, L., Sargent, D., Ford, R., Dancey, J., Arbuck, S., Gwyther, S., Mooney, M., Rubinstein, L., Shankar, L., Dodd, L., Kaplan, R., Lacombe, D., and Verweij, J., “New response evaluation criteria in solid tumours: Revised RECIST guideline (version 1.1),” *European journal of cancer* **45**, 228–247 (2009).
- [2] Moltz, J., Bornemann, L., Kuhnigk, J.-M., Dicken, V., Peitgen, E., Meier, S., Bolte, H., Fabel, M., Bauknecht, H.-C., Hittinger, M., Kießling, A., Püsken, M., and Peitgen, H.-O., “Advanced segmentation techniques for lung nodules, liver metastases, and enlarged lymph nodes in ct scans,” *IEEE Journal of Selected Topics in Signal Processing* **3**(1), 122–134 (2009).

- [3] Bornemann, L., Dicken, V., Kuhnigk, J.-M., Wormanns, D., Shin, H.-O., Bauknecht, H.-C., Diehl, V., Fabel, M., Meier, S., Kress, O., Krass, S., and Peitgen, H.-O., "OncoTREAT: a software assistant for cancer therapy monitoring," *International Journal of Computer Assisted Radiology and Surgery* **1**(5), 231–242 (2007).
- [4] Laidlaw, D. H., Fleischer, K. W., and Barr, A. H., "Partial-volume bayesian classification of material mixtures in MR volume data using voxel histograms," *IEEE Transactions on Medical Imaging* **17**, 74–86 (1998).
- [5] Salvado, O. and Wilson, D. L., "A new anisotropic diffusion method, application to partial volume effect reduction," in [*SPIE Medical Imaging*], **6144**(1), 614464 (2006).
- [6] Rousset, O. G., Ma, Y., and Evans, A. C., "Correction for partial volume effects in PET: Principle and validation," *The Journal of Nuclear Medicine* **39**, 904–911 (1998).
- [7] Bello, F., Colchester, A. C. F., and Röhl, S. A., "A generalised geometry and intensity based partial volume correction for magnetic resonance images," *Image Analysis and Processing* **1311/1997**, 428–435 (1997).
- [8] Rexilius, J. and Peitgen, H.-O., "Evaluation of accuracy in partial volume analysis of small objects," in [*SPIE Medical Imaging*], **6914**(1), 69144X (2008).
- [9] Kuhnigk, J.-M., Dicken, V., Bornemann, L., Bakai, A., Wormanns, D., Krass, S., and Peitgen, H.-O., "Morphological segmentation and partial volume analysis for volumetry of solid pulmonary lesions in thoracic CT scans," *IEEE Transactions on Medical Imaging* **25**(4), 417–434 (2006).
- [10] Dehmeshki, J., Ye, X., Amin, H., Abaei, M., Lin, X. Y., and Qanadli, S. D., "Volumetric quantification of atherosclerotic plaque in CT considering partial volume effect," *IEEE Transactions on Medical Imaging* **26**(3), 273–282 (2007).
- [11] Heckel, F., Moltz, J. H., Bornemann, L., Dicken, V., Bauknecht, H.-C., Fabel, M., Hittinger, M., Kießling, A., Meier, S., Püsken, M., and Peitgen, H.-O., "3D contour based local manual correction of tumor segmentations in CT scans," in [*SPIE Medical Imaging*], **7259**(1), 72593L (2009).